MEDDOCS Open Access Publisher

ISSN: 2578-8760

Journal of Nanomedicine

Open Access | Research Article

Nanoscale structural analyses on Rod Outer Segments (ROS) membranes and retina of bovine eye: 3D structure of photoreceptor nanodomains

Ilghar Orujalipoor[1,2]; Mustafa Erbakan[3]; Semra İde[4]*

[1]Department of Nanotechnology and Nanomedicine, Hacettepe University, Ankara, Turkey

[2]Alptek Engineering and Technological Systems A. S., Umraniye, 34774, Istanbul, Turkey

[3]Department of Biosystems Engineering, Bozok University, Yozgat, Turkey

[4]Department of Physics Engineering, Hacettepe University, Ankara, Turkey

***Corresponding Author(s): Semra İDE**

Department of Physics Engineering, Hacettepe University, Ankara, Turkey

Email: side@hacettepe.edu.tr

Received: Jan 15, 2020

Accepted: Mar 15, 2020

Published Online: Mar 19, 2020

Journal: Journal of Nanomedicine

Publisher: MedDocs Publishers LLC

Online edition: http://meddocsonline.org/

DOI: http://doi.org/10.33582/2578-8760/1018

Keywords: Retina; TEM; Rhodopsin; X-ray Scattering; SAXS; WAXS

Abstract

The present study aims nanoscopic observation and detection of rhodopsin (a G protein- coupled receptor) nanodomains in their native biological environment to investigate their kinematics related to the photocycle. In the first phase of the planned work, the retina segments were obtained from bovine eyeballs and different sample preparation methods were tested to identify the densely packed rhodopsin nanodomains.

Transmission Small- and Wide-Angle X-Ray Scattering (SAXS and WAXS) methods were used for nanoscale analyses of the prepared samples. The compact conformations of rhodopsin nanodomains in the structure of the native retina and the Rod Outer Segments (ROS) isolated from retina were elucidated. The related scattering data were used to reveal nanoscale morphologies and internal structures of the rhodopsin nanodomains. Nanostructure of rhodopsin within the intact retina was also directly identified to compare the rhodopsin structure in isolated ROS. Direct measurement of the retina reveals similar hierarchical structure defined by paracrystalline arrays suggesting that nanostructural features of rhodopsin domains.

The quantitative results indicate an inter-disk spacing of 30.00 nm and a bilayer thickness of 6.84 nm for the ROS membrane. 3D structure of the rhodopsin was also characterized by ellipsoidal globules including sizes of the main axes and electron densities. The results showed that SAXS-WAXS analyses are effective in monitoring the nanoscale bioactivation of rhodopsin in retina and the flexible cylinder model is in good coherence with the alpha-helical transmembrane domains of rhodopsin.

Cite this article: Orujalipoor I, Erbakan M, Ide S. Nanoscale structural analyses on Rod Outer Segments (ROS) membranes and retina of bovine eye: 3D structure of photoreceptor nanodomains. J Nanomed. 2020; 3(1): 1018.

Introduction

The receptor organ for vision is the eye. Being one of the most complex organs in the body, eye gives a sense of sight to many genera of animals allowing them to obtain information about their surroundings. This organ operates like a camera; light let on by the cornea is controlled by the pupil and is transformed into electrical signals by the retina and sent to the brain where the signals are interpreted into visual images [1]. The eye is composed of the eyeball, the optic nerves and the accessory structures such as conjunctivae, lacrimal apparatus and extraocular muscles. The eyeball has three distinct layers; the fibrous tunic (cornea and sclera), the vascular tunic (iris, ciliary body and choroid), the nervous tunic (retina). The retina which is the inner part of the eye, contains two major types of light-sensitive photoreceptor cells involved in vision: the rods and the cones. These photoreceptor cells respond to the different spectrum of the light due to different pigment molecules enabling them to transmit a signal that triggers a cascade of biochemical reactions. The signal is converted to electric pulses by the optic nerves and transmitted to the brain, which perceives it as vision [2].

Cone receptors contain three different cone opsins and respond to photons of different wavelengths, thus providing a basis for the color vision [3]. However, the rods are responsible for low-light (scotopic) monochromatic (black-and-white) vision. Rods are distributed throughout the retina, however there are none at the fovea and the blind spot. Rod density is greater in the peripheral retina than in the central retina. They work well in dim light, due to the distinct structure of their outer segments, which is responsible for the collection of the light photons. Rod outer segments (ROS) is composed of a plasma membrane and about one thousand of intracellular membrane disks stacked on top of one another. Disk membranes harbor abundant amount of a pigment protein called rhodopsin. The specific orientation of the ROS membrane disks (being contained in the cytoplasm and stacked in close neighborhood of each other) and high concentration of rhodopsin imparts low light sensitivity to rods. Rhodopsin is also known as visual purple because it absorbs green-blue light most strongly and appears purplish in color due to 11-cis retinal prosthetic group attached to the amino acid backbone [4]. Rhodopsin belongs to a highly specialized family of receptors called G protein-coupled receptors (GPCR), which detects photons in the ROS and mediates light initiated sensory signal as a transmembrane protein. GPCRs are of special importance, because they form one of the largest and the most diverse groups of receptor proteins [5,6]. Evolutionary adaptation to distinct environments has affected the selection of pigment isoforms, the level of pigment expression, the number of photoreceptor cell types, and the spatial organization of photoreceptors in animals [7]. While retinas of domestic mammals contain mostly rods, the retinas of domestic birds contain cones [2]. The number and ratio of rods to cones varies among species depending on whether the animal is primarily diurnal or nocturnal [8]. For example, the owls have a tremendous number of rods in their retina [9].

The outer segments of rod and cone photoreceptor cells have important biochemical roles for photo transduction. The visual transduction starts when the visual pigment rhodopsin located in ROS catches a light photon while it culminates in the closure of cyclic guanosine monophosphate depended ion channels located in the plasma membrane [10]. The changes in the ROS structure and the detailed morphological information obtained from the native ROS, particularly from different mammals, are of crucial importance to understand mechanisms underlying phototransduction and retinal dystrophies. The models, including micro-nano and molecular scale structural details of retinal dystrophies, can provide a method for testing various genetic and pharmacological therapies to combat diseases leading to blindness [11].

Quantitative considerations on retina, opsin macromolecules and their three-dimensional morphological analyses has seen much interest during last ten years. Especially modern experimental techniques and their informative guidance provide a better understanding of retina rod and cone structures and their biochemical properties [10-15]. Distances among the various membrane components, the proper distance between adjacent discs and distributions of rhodopsins therein are also very important and deterministic for phototransduction.

This study aims to quantitatively characterize nanoscopic bovine ROS and rhodopsin structures by X-ray scattering methods. The specific aim is extension of the experimental limits to detect the native rhodopsin structures in nanoscale.

Until the present research, structural characterizations of rhodopsin nanodomains in ROS were limited by imaging techniques such as Transmission Electron Microscopy (TEM), Scanning Electron microscopy (SEM) and tomographic techniques [16]. The native ROS disc membranes have rhodopsin dimers and contain densely packed rhodopsin molecules for optimal light absorption [14,17].

It is suggested that the organization principle of rhodopsin into nanodomains in mammalian ROS disc membranes is conserved acROS all vertebrate species [18]. Naturally how these photoreceptors are organized with respect to each other is still largely unknown in the electron density level. In a recent study, a native eye disc membrane has been adsorbed on mica and the structure has been visualized by Atomic Force Microscope (AFM) and consequently, the oligomeric organization of rhodopsin dimers has been defined in paracrystalline structural form [19-22].

On the other hand, rhodopsin arranged in dimers and oligomers in the vitrified ROS were also obtained by using the modern cryo-electron tomography method [23].

The paracrystalline arrays of the rhodopsin dimers in the surface of a native eye-disc membrane have been reported but their 3D shape, dimensions of the naturally possible paracrystalline arrays (in native retina and ROS structures) are still of a paramount interest for different mammalian species [22,24].

It is known that many collaborative techniques for the study of rhodopsin such as UV visible, fluorescence, ESR and Fourier-transform infrared (FTIR) spectroscopies are informative [25] for the atomic and molecular scaled structural details but the present study will supply nanoscale information to complete the missing scale on the native structure of bovine ROS and rhodopsin.

The present study is predicted to be beneficial for humans' future in space. As it is also known that the retinal damage in astronauts' eyes are very important for Human's space travel because of the negative repercussions of zero gravity. Our scientific target in our near future study will be related with nanoscopic detection and examination of the environmental physical response behaviours of retina and rhodopsin. Because, eyeballs

can be significantly reshaped and space conditions can create folds on the retina [26]. Our studies may generate new insights and hints about the preventive treatments just before the appearing vision problems of the most astronauts who spend more than a month in space.

Beside of zero gravity, the low air pressure effects on the retina and rhodopsin may be also kinetically investigated by using pressure and gravitation response time resolved SAXS-WAXS measurements. Of course, these analyses will be also supported by complementary methods [25]. So the wide range (molecular, nanoscopic and macroscopic) structural changes and the research and development studies on useful potential treatments may be easily followed and examined.

In this work, SAXS and WAXS analysis were first case carried out to directly detect nanoscopic structural contents the focused biological samples in their natural form without any purification and external effects.

Materials and methods

ROS Isolation and Sample Preparation

Fresh bovine eyes were obtained from Sincan Slaughter House, Ankara. SAXS and WAXS experiments on intact retina were performed immediately after the isolation of retina from dissected eyeballs. ROS preparation was conducted according to [27] with the following modifications. The retina segments obtained from bovine eyeballs were surgically prepared. The samples were divided into two groups. In the first day of the preparation, the first group of eye samples were dissected to isolate the retina by a pair of flat forceps. The isolated retinas were supplemented with 0.5 ml of an isotonic buffer (IB) containing 10 mM HEPES (pH adjusted to 7.4 with KOH), 115 mM NaCl, 2,5 mM KCl, 1 mM $MgCl_2$ and 1 mM DTT (added fresh) per retina. Then, the retina sample was vigorously shaken for 90 sec and centrifuged at 3,000 rpm for 10 min. The supernatant was filtered through a cheese cloth with 100 micron pore size and fixed in 4% formaldehyde (from a stock of 16% formaldehyde in IB) overnight at 4ºC. The buffer content of the sample was adjusted to 0.75M sucrose using a 2x stock in IB immediately prior to sucrose density centrifugation. The sample was centrifuged at 10,000 g for 10 min; the pellet is reserved and the supernatant was span again. The pellets from first and the second centrifugation step were combined and resuspended in 120 µL IB with 0.75M sucrose per retina.

In the second day of the preparation, the retinas was obtained the second group of fresh eye samples and supplemented with IB containing 1.5 M sucrose (0.5 ml/retina) to isolate ROS by vigorous shaking for 90 sec. Sucrose was added to IB so as to increase the detached ROS amount. The sample was centrifuged at 3,000 g for 10 min and the supernatant was filtered through a 100 micron pore-sized cheese cloth. The permeate was diluted 1:1 with IB to set the final sucrose concentration to 0,75 M. The rest of the sample preparation procedure was the same as the first group of samples.

The step gradient was prepared by carefully overlaying 3 ml of 40% sucrose in IB, 4 mL of 35% sucrose in IB, 4 mL of 30% sucrose in IB and 4 mL of 25% sucrose in IB in a 15,6 mL ultracentrifuge tube, respectively. 0.5 ml from fixed or fresh samples was added on top of the step gradient and the centrifugation was carried out for 90 min at 105000 x g using a swing bucket rotor in BECKMAN XL-90 Ultracentrifuge. ROS band was carefully collected between 30% and 35% sucrose layers and diluted 1:1 with IB. ROS sample was centrifuged at 10,000 g for 10 min and the supernatant was discarded. The pellet was resuspended in 10 mM HEPES (pH=7.4), 1 mM DTT (added fresh) and 0.1 mM PMSF (added fresh). TEM and SAXS/WAXS experiments were conducted immediately after the ROS preparation to minimize the deterioration of the samples.

TEM

Transmission electron microscopy measurements of the isolated ROS samples were conducted via FEI Technai G2 transmission electron microscope. 3.5 µL of isolated ROS sample was pipetted to form a sessile drop on carbon coated copper grid and incubated for 30 seconds. The extra sample was blotted on Whatman filter paper. The sample side of the copper grid was contacted with the top of a 50 µL of IB droplet which was spotted on a parafilm sheet and the extra buffer was blotted on filter paper. The process was quickly repeated for 4 times. Two drops of 8 µL uranyl acetate solution (2%) were spotted on a parafilm. The sample side of the copper grid was contacted in the first uranyl acetate droplet and blotted instantly. The grid was contacted with the second uranyl acetate spot and incubated sample side down for 20 seconds and blotted. The grids were air dried briefly prior to TEM measurements.

X-Ray scattering

SAXS-WAXS experiments of the samples were performed by a HECUS X-ray Systems (Graz, Austria). Different sample holders were used to measure the samples. Quartz capillary tubes with a diameter of 1.5 mm were used for solutions and a stainless steel thin polymeric sheet window was used for retina. X-ray exposure time was 100 seconds for each sample to avoid radiation damage effect of X-rays (CuK_α wave length of 1.542 Å). The experiment was performed at 21°C with an X-ray generator operating at 50kV and 40mA (2kW). Two 1D–position sensitive detectors each containing 1024 channels with width of 54.0 µm was used for detection of scattered X-rays in the small- and wide-angle regions. The covered momentum transfer range (q-range) was $0.004 \le q \le 0.5$ Å^{-1}, where $q=4\pi\sin(\theta)/\lambda$. The forward scattering I(0) and the radius of gyration (R_g) were calculated using the Guinier approximation, which assumes that at the limited small angles ($q < 1.3/R_g$), the intensity is approximated as $I(q) = I(0) \exp[-(qR_g)^2/3]$. GNOM and Igore Pro programs [28], [29] were used to calculate the pair-distance distribution function P(r), from which the maximum particle dimension (D_{max}) and R_g were determined.

SAXS data based modeling

The best fitted model for the macromolecular complexes was triaxial ellipsoid. Two numerical integrations have to be performed in order to get the orientational average in the nanoscale modeling of the tri-axial ellipsoids [29,30].

The form factor for the triaxial ellipsoid with the semi axes of a,b,c can be generalized as follows.

$$P(q) = \frac{scale}{V_{el}} \int_0^1 \int_0^1 \phi^2 \left\{ q[a^2 \cos^2(\pi x/2) + b \sin^2(\pi x/2)(1-y^2) + c^2 y^2)]^{1/2} \right\} dxdy$$

Where the function of ϕ(x), the volume of ellipsoid V_{el} and radius of gyration R_g are defined as respectively.

$$\phi^2(x) = 9\left(\frac{\sin x - x\cos x}{x^3}\right)^2, V_{el} = \frac{4\pi}{3}abc, R_g^2 = \frac{a^2+b^2+c^2}{5}$$

Employing dummy residues and constraints were provided within the SAXS profiles to obtain *ab initio* structure restoration including shape and domain structure related to macromolecular complexes. So, the 3D shapes of rhodopsin dimers were restored using the DAMMIN program using rigid body refinement [31].

Results & discussion

ROS isolation and sample preparation

As detailed in materials and methods section, samples that were used in TEM and SAXS/WAXS experiments were prepared from fresh eyeballs. Only one set of samples were fixated in 4% formaldehyde overnight after ROS detachment was achieved Figure 1. shows the ROS preparation steps: dissection of the eyeball to obtain the retina), detachment of the ROS from other retina components, sucrose gradient centrifugation of photoreceptor components and the isolated ROS

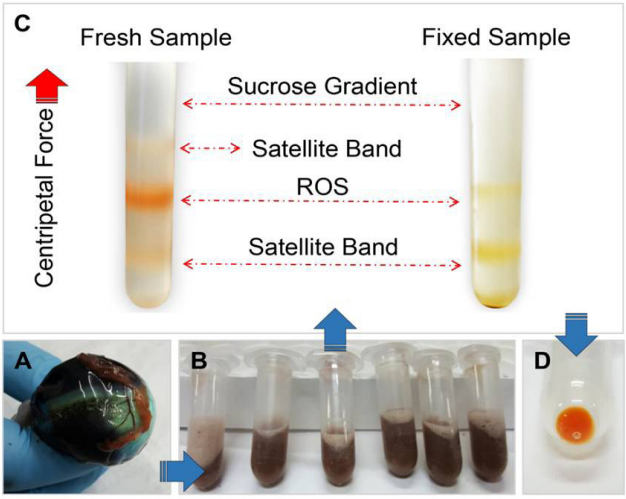

Figure 1: Separated bands of the treated fresh and fixed retina samples (up) after centrifugation. (A) Dissected eyeballs, (B) ROS detached from other layers of retina, (C) ROS separated by sucrose density centrifugation, (D) Isolated ROS. Fresh samples maintained red color of 11-cis retinal, while fixation seemed to promote the all-trans form even though the overnight incubation was carried out in dark at 4ºC.

Considering that osmotic pressure exerted on ROS by high sucrose concentration in centrifugation buffer might distort the 3D structure of the ROS and rhodopsin; one set of ROS samples was fixated using 4% formaldehyde prior to sucrose density centrifugation to diminish the structural deformations. ROS band from fresh samples had intact red color of 11-cis retinal implying that the majority of the rhodopsin molecules did not interacted with light. However, ROS band from fixated samples had the characteristic yellow color of all-trans retinal hinting that rhodopsin interacted, with light during the sample preparation step, although the samples were kept in dark at 4 ºC during the fixation process. Comparing the satellite band and ROS band intensities of fresh and fixed samples, we note that the level of ROS detachment from inner segment of rods and other retina layers was significantly higher in fresh samples, which can be attributed to the high shear on rod cilium due to the increased osmotic pressure in IB supplemented with 1,5M sucrose compared to IB without sucrose for fixated samples.

TEM

Quality and integrity of ROS preparations were evaluated by negative staining TEM. Figure 2 shows that high sucrose concentrations in centrifugation buffer distorted the original shape of the ROS due to osmotic pressure difference across the plasma membrane. Membrane disks separated from a ruptured ROS, possibly due to osmotic stress, are seen in the TEM image in Figure 2B. Although this sample is not suitable for evaluation of the geometrical factors of ROS and the intracytoplasmic disks within, it is still useful to study the native states of rhodopsin. The light trigged (11 cis- and all trans-) isomerization of retinal and 3D morphological changes in the structure of rhodopsins may be easily detected by SAXS analyses. The isomerization of retinal between 11-cis retinal (red) to all-trans retinal (yellow) is accompanied with a change in the absorption spectrum.

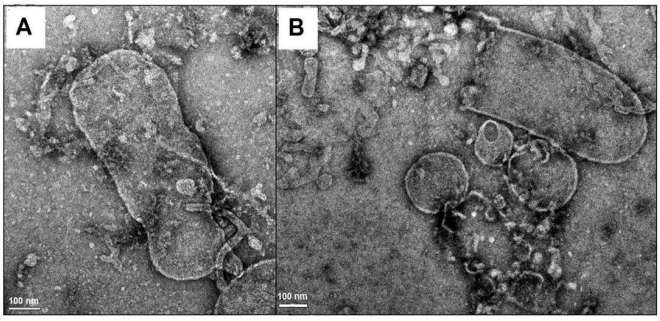

Figure 2: TEM images of ROS isolated from fresh bovine eyes (scales bars represent 100 nm).

Figure. 3 shows TEM images of ROS samples fixed by 4% formaldehyde prior to sucrose density centrifugation. Fixation seemed to reinforced the structural integrity of the ROS. TEM image is informative in terms of measurement and determination of the dimensions and geometry of the ROS. The connecting cilium and transition zone [32] between outer and inner segments is also seen in Figure 3.

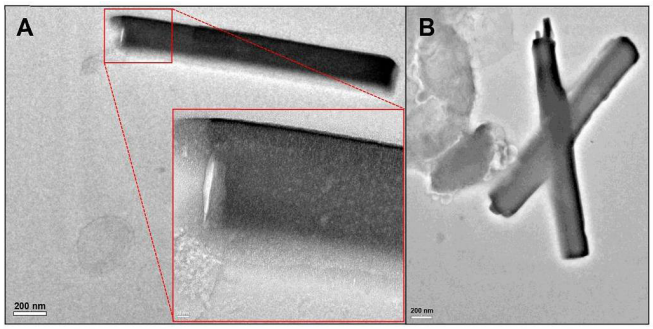

Figure 3: TEM views of fixed ROS with scales of 200 nm

According to microscopic evaluations, the determined structural parameters were given in Table 1. We measured smaller values respect to the previously reported parameters [33], [34]. Especially for the length of ROS from fresh sample were smaller than that of the fixed sample. The reason for this observation may be the distortions caused by centrifugal compaction and osmotic pressure.

Table 1: The measured geometrical parameters of the ROS

Samples	Length of the ROS (nm)	Diameter of the ROS (nm)	Diameter of cilium/ transition zone (nm)	Diameter of the disk membrane (nm)
Fresh	739 ± 7 nm	289± 7 nm	56± 7 nm	199± 7 nm
Fixed	1913 ± 13 nm	278± 13 nm	77± 13 nm	-

SAXS-WAXS

The obtained SAXS (Figure 4A, 4B and 4C) and WAXS (Figure 4D) profiles were given in Figure 4. According to the qualitative comparison of the illustrated data, it can be said that nanostructured content have more scattered and distinguishable contributions to the data in the profiles of fresh origin compared to that of fixed one. The more recordable and clear humps in Figure 4 is the evidence of these nanoscopic structural contents because of the expected scattered data. The SAXS profiles related to Band 2 were also illustrated together in the same figure (Figure 4) which has hints of the possible crystalline arrangements for fresh samples.

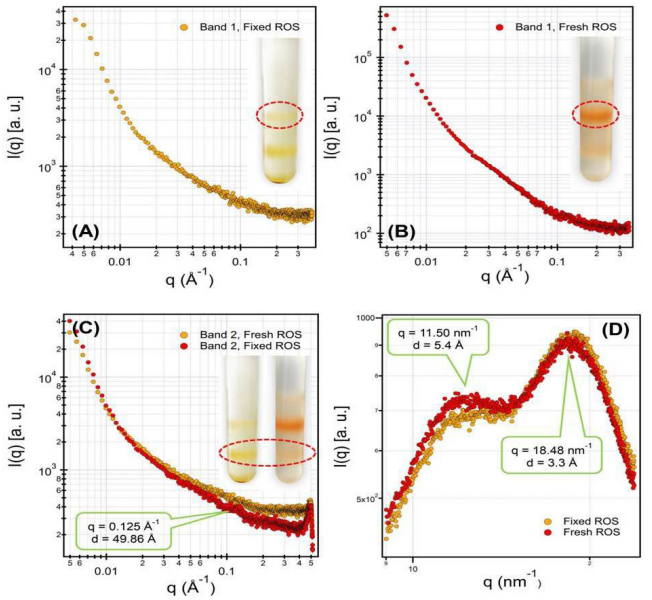

Figure 4: 1D-SAXS profiles of Band 1. and Band 2 isolated after sucrose density centrifugation. Band 1 includes ROS and while Band 2 contains inner segments attached to ROS's (4A, 4B and 4C) and WAXS data of Band 1 from both samples (4D)

In this part of the study, nanoscale 3D folding of rhodopsin in bovine retina and their native states were quantitatively investigated by using small and wide angle X-ray scattering (SAXS/WAXS) analyses. Three axial ellipsoid model (Figure 5) was used in fitting process of the data to describe rhodopsin macromolecules and rhodopsin nanodomains. The WAXS data did not include significant peaks for Band 2 while Band 1 has two humps possibly related to molecular scope-crystalline like ordering.

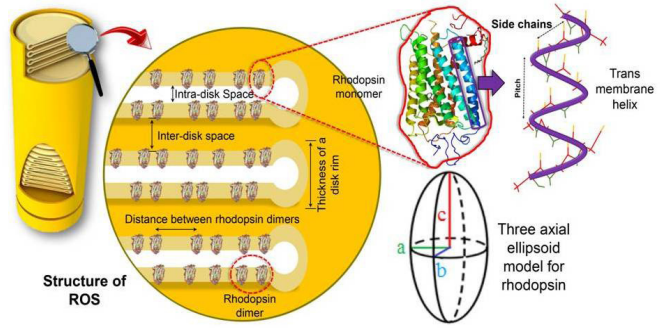

Figure 5: The nanoscale structural content of a ROS, crystalline arrays of rhodopsins (GPCRs), the 3-axial ellipsoid model of rhodopsin and the view of a transmembrane helix.

According to the fitting process, all structural parameters mentioned in Section 2.3 were refined to reach at the acceptable χ^2 values. As seen in Table 2, SAXS is a very sensitive and effective method to focus on rhodopsin domains and the ROS structures are very stable together with rhodopsin content.

Table 2: The measured geometrical parameters of the ROS

Refined Parameters	Retina	ROS (Normal)	ROS (Fixed)
Scale	0.9	1.7	0.9
Small axis, a(Å)	18.0	18.2	18.8
Middle axis, b(Å)	24.9	24.6	25.6
Long axis, c(Å)	39.7	39.5	39.6
SLD, Ellipsoid ($Å^{-2}$)	$8.2x10^{-5}$	$8.3x10^{-5}$	$8.0x10^{-5}$
SLD, Solvent ($Å^{-2}$)	$9.9x10^{-6}$	$9.8x10^{-6}$	$9.7x10^{-6}$
Bkg (cm^{-1})	60.1	51.1	54.5

SLD: Scattering Length Density; Scale: Multiplayer Related with the Nanodomain Number Per Scattered Volume; BKD: background scattering

In the other phase of the SAXS analyses, the scattering curves were used to construct low-resolution 3D SAXS models (Figure 5) using DAMMIN program. The volume distributions were also obtained with the same data and by using the other software.

The compact domains adopt different 3D conformations in the sub-ensemble. The one selected sub-ensemble (from fresh samples) corresponds to two (dimer) conformers which have similar shape and close distribution because of more paracrystalline arrayed rhodopsin content in fresh ROS. A compact conformer with interdomain interactions was obtained for fixed sample and the extended structural content is also including smaller nanodomains as evidenced by volume distribution for fixed samples.

At the end of the present work, the detailed 3D nanoscale structure and heterogeneous nanodomains including dimeric rhodopsin macromolecules were obtained as seen in Figure. 6-7. It was determined that the obtained *ab-initio* model also supported paracrystalline arrays in the structural content of the native retina. The possible unit cell of the paracrystalline array was also obtained in DAMMIN view for fresh sample (Figure 7). The previously decelerated model also supports that the newly obtained model in the present work by using SAXS data and paracrystalline array.

The PDDs (Pair Distance Distributions) of the nanoglobules in the structural contents of fresh retina, fresh ROS and fixed ROS samples were determined by Moore's Indirect Fourier analyses [29] as seen in Figure 8. These distributions are also the evidence of the disk membrane and rhodopsin nanodomains with several observed humps. The presence of the other macromolecules in the structural content of retina can cause X-ray scattering, as well. The big and wide hump is including these structures. But crystalline and paracrystalline ordered layers related with ROS structure are causing dominant and distinguishable scattering effects in the data. Small and lamellar humps are related with rhodopsin dimers. These humps are more distinguishable in the PDDs of the ROS as expected because of the separated disk contents.

The PDDs (Pair Distance Distributions) of the nanoglobules in the structural contents of fresh retina, fresh ROS and fixed ROS samples were determined by Moore's Indirect Fourier analyses [29] as seen in Figure 8. These distributions are also the evidence of the disk membrane and rhodopsin nanodomains with several observed humps. The presence of the other macromolecules

in the structural content of retina can cause X-ray scattering, as well. The big and wide hump is including these structures. But crystalline and paracrystalline ordered layers related with ROS structure are causing dominant and distinguishable scattering effects in the data. Small and lamellar humps are related with rhodopsin dimers. These humps are more distinguishable in the PDDs of the ROS as expected because of the separated disk contents.

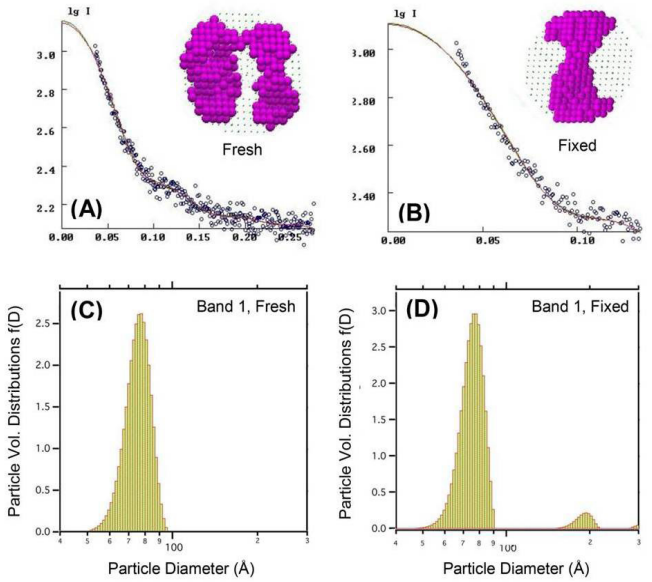

Figure 6: SAXS shape reconstitution and scattering envelopes computed by using DAMMIN (6A and 6B). *Ab initio* SAXS model (Scattering envelope) for rhodopsin nanograins were generated by fitting of single-conformation to experimental scattering data. The obtained average SAXS models were shown by pink residue balls (6B). The volume distributions related with fresh and fixed samples were also given in the figure 6C and 6D.

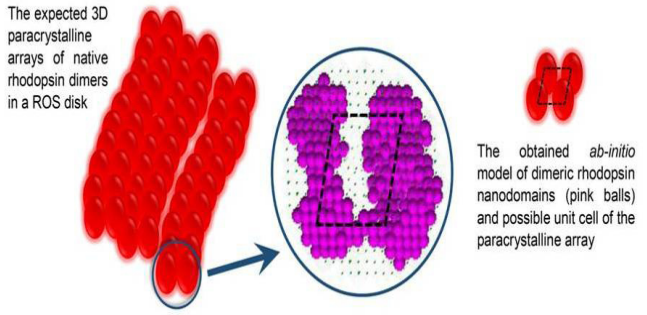

Figure 7: Correlation between the expected and densely packed paracrytalline lattice [35] and the obtained 3D model of dimeric rhodopsin formations.

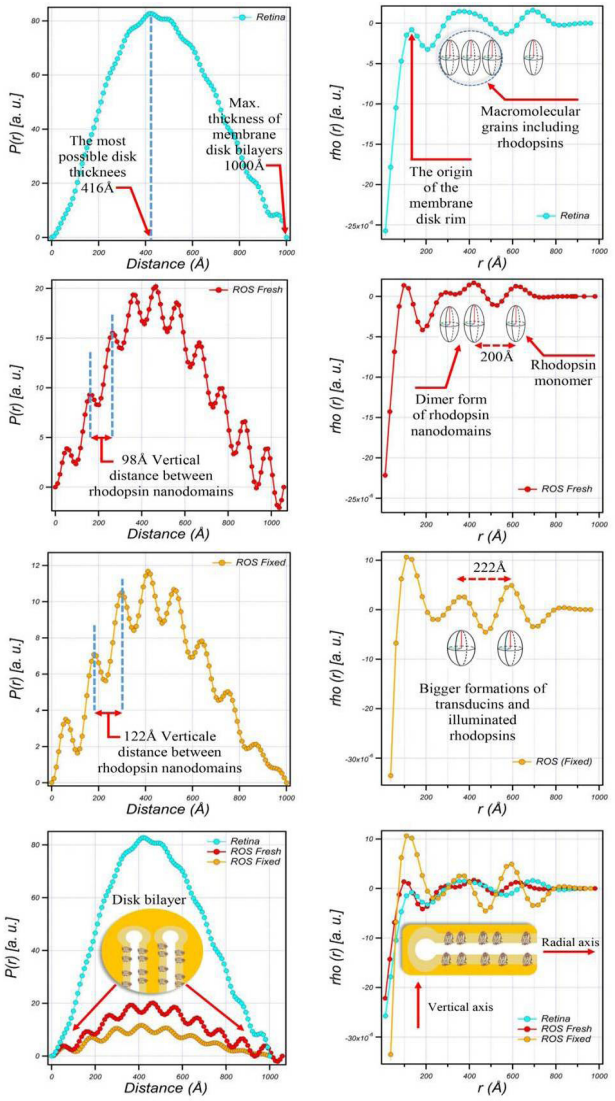

Figure 8: Correlation between the expected and densely packed paracrytalline lattice [35] and the obtained 3D model of dimeric rhodopsin formations.

The quantitative detection of different shaped and sized nano aggregations by using the illustrated PDDs (Figure 8) are very informative for nanostructural contents including membranous discs and rhodopsin globules.

Two humps were obtained which were possibly related with the rim regions of ROS disk membranes including lamellar bilayers in the PDD of native retina.

The significant correlation between PDDs evaluations and structural model of ROS can be explained by Figure 8 All structural parameters defined by disc diameter, the mean distance between discs, intra-disc space, thickness of membrane bilayer and rhodopsin size can be measured by PDDs analyses as seen in Figure 8**.**

When the X-ray beam scattered from retina samples (in transmission mode), strong well-oriented histogram peaks were observed in PDDs as an evidence of lamellar aggregations related with the neighboring disk membranes in ROS. This lamellar stacking, with a periodicity of 30.0 nm (300 Å), originates in a linear arrangement of disk membranes in the outer segment of retinal rod. The similar observations have been also recorded in the previous published studies for isolated mouse eyeballs

(30.4 nm) and the frog eye retinal rod (29.3 nm) [36].

As it is seen in WAXS profile (in Figure .4(D)), two crystalline peaks were obtained. The first peak was appeared at q=11.50 nm^{-1} (d=2π/q=5.40 Å) and the second peak at q=18.48 nm^{-1} (d=3.3Å) most likely demonstrates the pitch value of the helical structure and the spacing between side chains inside the alpha-helices, respectively. These results should be confirmed by WAXS analyses on the isolated rhodopsin macromolecules which is a part of our next planned research program. Because macromolecular content of the focused biological samples are very rich and small molecular contributions to the scattering data actually more recordable with more intense peaks which are appeared in WAXS range [37].

Conclusion

At the end of the study we may summarize the obtained results as follows,

- It is wanted that biological sample preparation procedures should not change the native content of the samples to investigate the macromolecular, nano and microscale structures. With this work, it was shown that rhodopsin structures may be investigated by using native fresh retina samples and SAXS-WAXS methods without any chemical effect.
- The nanoscopic views for the more realistic structures related with photoreceptor cells are giving very important structural information about

i- 3D geometrical parameters of the folded rhodopsin inside of the ROS membrane disks.

ii- The most possible 3D dimer formation of the rhodopsin nano domains and their paracrystalline arrays

iii- The thickness of a disk rim

iv- The interplanar disk space of the membrane disks, etc.

Beside of fundamental and conventional scattering data evaluation [38], indirect Fourier Analyses [28], [31] and the determined PDDs were also helpful to obtain real space nanostructure of the studied biological samples. The obtained parameters related with ROS of bovine retina can be summarized as follows,

-The distance of inter membranes is 83.3 Å,

-The thickness of membrane bilayers is 68.4 Å,

-The distance of the alpha-helices transmembranes side chains is 3.3 Å

- Separation of the ROS and purification of rhodopsins from the disk membranes are not necessary to investigate light effects, therapy process and external bio-chemical and physical effects on photoreceptor cells. So, the study on the function of the rhodopsin and associated retinal diseases may be easier by SAXS and WAXS analyses.

SAXS evaluations suggest that the obtained structural parameters are directly related with the native organization of rhodopsins. The implications of the similar type of organization have begun to be considered computationally and experimentally [17], [18]. The obtained structural framework should be incorporated into the current view of phototransduction in photoreceptor cells and the determinants and role for this type of organization should be examined in more detail by using all of the complementary methods.

On the other hand, the light effect on rhodopsin structure will be also investigated and light illumination induced structural changes on retina will be also examined with SAXS in the future work. When the eyes were illuminated with intense light through cornea, the size (especially, a and b parameters of the ellipsoidal model) of rhodopsin will be increased because of all-trans retinal form. Beside of the size of the rhodopsin, the other structural parameters will be also big probably affected because of transformation from cis-retinal to trans-retinal form. Briefly, it may be said that as general conclusion, this work provides an attractive strategy for the nanoscopic detection of ROS and rhodopsin macromolecules. The different illness-treatment and physical- chemical effects on the retina may be followed in nanometric scale by using X-Ray scattering methods.

As mentioned in the introduction, the scientific vision of the present study will include and be related to complementary methods in our next level works. Experimental applications of these methods especially will initially be planned on low/high air pressure response kinetic measurements. So the results of these planned studies will be potentially useful for the eye vision problems of astronauts, sailors, researchers working in space or under the sea.

Acknowledgements

Authors would like to thank the authorities of the Department of Molecular Biology and Genetics at Bilkent University, because of the usage of the high-speed centrifugation system.

References

1. Guyton DL. Sights and Sounds in Ophthalmology. Ocular motility and Binocular vision. 1989.
2. Reece WO, Functional Anatomy and Physiology of Domestic Animals, 4th ed. Iowa, USA: Wiley-Blackwell. 2009.
3. McBee JK, Palczewski K, Baehr W, Pepperberg DR. Confronting complexity: The interlink of phototransduction and retinoid metabolism in the vertebrate retina. Prog. Retin. Eye Res, 2001; 20: 469-529.
4. D Purves, Neuroscience Third Edition. 2004: 3.
5. Liu DG, Chang CH, Liu CY, Chang SH, Juang JM, et al. A dedicated small-angle X-ray scattering beamline with a superconducting wiggler source at the NSRRC. J Synchrotron Radiat. 2008; 16: 97-104.
6. Vaidehi N, Floriano WB, Trabanino R, Hall SE, Freddolino P, et al. Prediction of structure and function of G protein-coupled receptors. Proc Natl Acad Sci. 2002; 99: 12622-12627.
7. Jacobs GH. The distribution and nature of colour vision among the mammals. Biol Rev Camb Philos Soc. 1993; 68: 413-471.
8. Rojas LM, McNeil R, Cabana T, Lachapelle P. Behavioral, morphological and physiological correlates of diurnal and nocturnal vision in selected wading bird species. Brain Behav Evol. 1999; 53: 227-242.
9. Braekevelt CR. Fine structure of the retinal photoreceptors of the great horned owl (Bubo virginianus). Histol Histopathol. 1993; 8: 25-34.
10. Nickell S, Park PSH, Baumeister W, Palczewski K. Three-dimensional architecture of murine rod outer segments determined by cryoelectron tomography. J Cell Biol. 2007; 177: 917-925.

11. Batten ML, Imanishi Y, Tu DC, Doan T, Zhu L, et al. Pharmacological and rAAV gene therapy rescue of visual functions in a blind mouse model of leber congenital amaurosis. PLoS Med. 2005; 2: 1177-1189.

12. Chang B, Hawes NL, Hurd RE, Davisson MT, Nusinowitz S, et al. Retinal degeneration mutants in the mouse. Vision Res. 2002; 42: 517-525.

13. Dalke C, Graw J. Mouse mutants as models for congenital retinal disorders. Experimental Eye Research. 2005; 81: 503-512.

14. Fotiadis D, Liang Y, Filipek S, Saperstein DA, Engel A, et al. Atomic-force microscopy: Rhodopsin dimers in native disc membranes. Nature. 2003; 421: 127-128.

15. Kawamura S, Gerstung M, Colozo AT, Helenius J, Maeda A, et al. Kinetic, energetic, and mechanical differences between dark-state rhodopsin and opsin. Structure. 2013; 21: 426-437.

16. Hirata A, Yamamoto S, Okinam A. Use of an Ophthalmic Visco-surgical Device for Experimental Retinal Detachment in Rabbit Eyes. J Funct. Biomater. 2013; 4 :6-13.

17. Malmerberg E, Bovee-Geurts PHM, Katona G,Deupi X, Arlund D,et al. Conformational activation of visual rhodopsin in native disc membranes. Sci Signal. 2015; 8: 26–26.

18. Rakshit T, Senapati S, Sinha S, Whited AM, Park PSH. Rhodopsin Forms Nanodomains in Rod Outer Segment Disc Membranes of the Cold-Blooded Xenopus laevis. PLoS One. 2015; 10: e0141114.

19. Fotiadis D, Liang Y, Filipek S,Saperstein DA, Engel A, et al. Atomic-force microscopy: Rhodopsin dimers in native disc membranes. Nature. 2003; 421: 127-128.

20. Fotiadis D, Liang Y, Filipek S, Saperstein DA, Engel A, et al. The G protein-coupled receptor rhodopsin in the native membrane. FEBS Lett. 2004; 564: 281-288.

21. Buzhynskyy N, Salesse C, Scheuring S. Rhodopsin is spatially heterogeneously distributed in rod outer segment disk membranes. J Mol Recognit. 2011; 24: 483-489.

22. Whited AM, Park PSH. Nanodomain organization of rhodopsin in native human and murine rod outer segment disc membranes. Biochim Biophys Acta - Biomembr. 2015; 1848: 26-34.

23. Gunkel M, schoneberg J, Alkhaldi W, Irsen S, Noe F, et al. Higher-order architecture of rhodopsin in intact photoreceptors and its implication for phototransduction kinetics. Structure. 2015; 23: 628-638.

24. Tanuj Sapra K, Park PSH, Filipek S, Engel A, Millller DJ, et al. Detecting molecular interactions that stabilize native bovine rhodopsin. J Mol Biol. 2006; 358: 255-269.

25. Klaassen CHW, Bovee-Geurts PHM, Decaluwé GLJ, Degrıp WJ. Large-scale production and purification of functional recombinant bovine rhodopsin with the use of the baculovirus expression system. Biochem J. 1999; 342: 293.

26. Stenger MB, Tarver WJ. Risk of Spaceflight Associated Neuro-ocular Syndrome (SANS). Houston, Texas. 2017.

27. Koch KW, Lambrecht HG, Haberecht M, Redburn D, Schmidt HH. Functional coupling of a Ca2+/calmodulin-dependent nitric oxide synthase and a soluble guanylyl cyclase in vertebrate photoreceptor cells. EMBO J. 1994; 13: 3312-3320.

28. Svergun DI. Determination of the regularization parameter in indirect-transform methods using perceptual criteria. J Appl Crystallogr.1992; 25: 495-503.

29. Kline SR.Reduction and analysis of SANS and USANS data using IGOR Pro," J. Appl. Crystallogr. 2006; 39: 895–900.

30. Pedersen JS. Analysis of small-angle scattering data from colloids and polymer solutions: modeling and least-squares fitting. Adv Colloid Interface Sci. 1997; 70: 171-210.

31. Svergun DI. Restoring low resolution structure of biological macromolecules from solution scattering using simulated annealing. Biophys J. 1999; 76: 2879-2886.

32. Rachel RA, Li T, Swaroop A.Photoreceptor sensory cilia and ciliopathies: focus on CEP290, RPGR and their interacting proteins. Cilia. 2012; 1: 22.

33. Mason WT, Biochemistry and physiology of visual pigments. Newyork: Springer Verlag, 1972.

34. Bauer P. Photoreceptors and Calcium (Advances in Experimental Medicine and Biology). 1 st. New York: Kluwer Academic/Plenum Publishers. 2002.

35. Liang Y, Fotiadis D, Filipek S, Saperstein DA, Palczewski K,et al. Organization of the G protein-coupled receptors rhodopsin and opsin in native membranes. J Biol Chem. 2003; 278: 21655-21662.

36. Yagi N, Matsuo T, Ohta N. An X-ray diffraction study on a single rod outer segment from frog retina. J Synchrotron Radiat. 2012; 19: 574-578.

37. Howard GC, Brown WE, Auer M. Imaging Life: Biological Systems from Atoms to Tissues, 1st ed. New York: Oxford University Press. 2014.

38. Feigin LA, Svergun DI, Structure Analysis by Small Angle X-ray and Neutron Scattering. New York: Plenum Press. 1987.